Organic Electronics 13 (2012) 2063–2074

Contents lists available at SciVerse ScienceDirect

Organic Electronics

journal homepage: www.elsevier.com/locate/orgel

Metallophthalocyanine and Metallophthalocyanine–fullerene complexes as potential dye sensitizers for solar cells DFT and TD-DFT calculations

A.S. Shalabi *, S. Abdel Aal, M.M. Assem, K.A. Soliman

Department of Chemistry, Faculty of Science, Benha University, Benha, P.O. Box 13518, Egypt

ARTICLE INFO

Article history:
Received 19 April 2012
Received in revised form 3 June 2012
Accepted 9 June 2012
Available online 2 July 2012

Keywords:
Phthalocyanine
Fullerene
Dye sensitizers
Solar cells
DFT calculations

ABSTRACT

The geometries, electronic structures, polarizabilities and hyperpolarizabilities, and UV–vis spectra of metallophthalocyanine dyes and metallophthalocyanine–fullerene supramolecules are investigated by using density functional theory (DFT) and time dependent density functional theory (TD-DFT) calculations. The results reveal that the metal and the tertiary butyl groups of the dyes are electron donors, and the phthalocyanine rings are electron acceptors. The electron donating power of (La) is significantly greater than that of (Sc). For dyes, the highest occupied molecular orbitals (HOMOs) are π orbitals localized over the phthalocyanine rings, away from the tertiary butyl groups, and the lowest unoccupied molecular orbitals (LUMOs) are π^* orbitals localized over the central metal atoms. The HOMOs of the dyes fall within the $(TiO_2)_{60}$ and $Ti_{38}O_{76}$ band gaps, and support the issue of typical interfacial electron transfer reaction. The resulting potential drop of the supramolecule $LaPc.C_{60}$ increases by ca. 22.86% under the effect of the tertiary butyl groups. This significant increase in the potential drop indicates that the tertiary butyl complexes could be a better choice for the robust operation of the molecular rectifiers. The introduction of metal atom and tertiary butyl groups to the phthalocyanine moiety leads to a stronger response to the external electric field, and induces higher photo-to-current conversion efficiency. This also shifts the absorption in the dyes and makes them potential candidates for harvesting light in the entire visible and near IR region for photovoltaic applications. It is also observed that the high spin state complex Sc(4)Pc could not be a potential candidate for harvesting light in the former region of spectrum.

1. Introduction

Dye sensitized nanocrystalline semiconductor based solar cells (DSSC) developed by Hagfeldt and Gratzel [1] are of immense interest as energy sources. DSSCs are promising in terms of efficiency and low cost [2]. In a dye-sensitized solar cell, an organic dye adsorbed at the surface of an inorganic wide band gap semiconductor is used for absorption of light and injection of the photoexcited electron into the conduction band of the semiconductor. The research on dye-sensitized solar cells gained considerable impulse, when Hagfeldt and Gratzel [3] greatly improved the interfacial area between the organic donor and inorganic acceptor by using nanoporous titanium dioxide (TiO_2). On the other hand, there has been considerable effort to find dye sensitized solar cells based on organic donor and fullerene acceptor. Many fullerene-based supramolecules have been proposed as potential organic photovoltaic devices, with their electrochemical and photo electrochemical properties measured under light illumination π-electron system, whereas fullerene is good π-electron acceptor which can be connected with other organic molecules. A phthalocyanine–fullerene-based supramolecular system is therefore a potential material candidate for a photovoltaic cell due to its large and flexible absorption combined with electrical properties similar to an inorganic semiconductor.

As far as theoretical investigations of dye sensitized solar cells are concerned, Mizuseki et al. [4] investigated the

* Corresponding author. Tel.: +20 100 5211681; fax: +20 2 24188738.
E-mail address: asshalabi@hotmail.com (A.S. Shalabi).

1566-1199/$ - see front matter © 2012 Elsevier B.V. All rights reserved.
http://dx.doi.org/10.1016/j.orgel.2012.06.028

geometric and electronic structure of phthalocyanine–fullerene supramolecule by using *ab initio* quantum mechanical calculations. Their results suggest that the lowest unoccupied molecular orbital (LUMO) state of this supramolecule is localized on the fullerene and the highest occupied molecular orbital (HOMO) state is localized on half of the phthalocyanine. Majumder et al. [5] investigated theoretically several donor(n-type)–spacer–acceptor(p-type) polyphenyl-based conjugated molecules. Their results suggest that the potential difference of the di-substituted rectifier complex is greater than that of the mono-substituted. Rong et al. [2b] investigated the geometries, electronic structures, polarizabilities and hyperpolarizabilities, and UV–vis spectra of several organic dye sensitizers by using DFT and TDDFT calculations. They reported that the polarizabilities of the dyes depend on the length of the conjugated bridge, the UV–vis spectra are assigned to $\pi \rightarrow \pi^*$ transitions, and the interfacial electron transfer is due to an electron injection processes from excited dyes to semiconductor conduction band. Mosurkal et al. [6] modeled acridine dyes in an attempt to clarify the effects of chemical structure on the longest wavelength absorption and provide insight into the performance of the dyes as sensitizers in DSSCs. Sun et al. [7] studied the geometrical structures, ionization potentials, electron affinities, reorganization energy, and UV–vis spectra of benzothiadiazole-based linear and star molecules by using DFT methods. They reported that the diethynyl groups improve the charge transfer character and extend the absorption wavelength towards the range with the maximum photon flux. Zhang et al. [8] carried out DFT and TD-DFT calculations to comparatively describe the molecular structure, molecular orbital energy gaps, atomic charges, Infrared (IR) and Raman (R), and UV–vis spectra of 1,6,15,22-tetra phthalocyanine-lead complexes. They found that substitution of bulky alkoxy groups at the nonperipheral positions of the phthalocyanine ring adds obvious effect to the molecular structure of phthalocyaninato lead compounds by deflecting the isoindole units in the direction that the isoindole units extends and distorting them in the C_4 axis direction due to the steric hinderance.

Phthalocyanine has good electron-donating properties and fullerene is a good π-electron acceptor. Both molecules can be connected together [9]. In the present study the geometries, electronic structure, polarizabilities and hyperpolarizabilities, and UV–vis spectra of phthalocyanine, metallophthalocyanine, and metallophthalocyanine tetra substituted tertiary butyl dyes as well as phthalocyanine–fullerene, metallophthalocyanine–fullerene, and metallophthalocyanine tetra substituted tertiary butyl–fullerene supramolecules are investigated by using DFT and TD-DFT calculations in order to understand the sensitized mechanisms and the factors that control the photo conversion efficiencies. Phthalocyaninato scandium and lanthanum compounds are selected to be representatives of transition metal and rare earth complexes.

2. Computational details

The self consistent field Hartree–Fock level (HF) with the smaller (LANL2MB) basis set were used for the optimized geometries of structural variables of the dyes, and for optimizing the distances between the dyes and fullerenes in the supramolecules to save computation time. The computations were then refined by single point energy calculations with the larger (SDD) basis set, and the DFT level for property predictions. The LANL2MB basis set places STO-3G on first row atoms, and Los Alamos ECP plus MBS on Na-La, Hf-Bi. The SDD basis set places Dunning/Huzinaga full double zeta D95 up to Ar, and Stuttgart/Dresden ECPs on the remainder of the periodic table.

The density functional theory calculations were performed by using Becke's three-parameter exchange functional B3 with LYP correlation functional [10]. The B3LYP hybrid functional has been chosen since it provides a rather accurate description of metal interactions. Hybrid functionals such as B3LYP provides a fair indication of the relative energies, and in some cases the resulting differences between the experimental values and the calculated ones can be considered a systematic error [11]. B3LYP correctly reproduce the thermochemistry of many compounds including transition metal atoms [12] and ensures a correct description of the electronic ground state of first row transition metal atoms and a reasonable description of the energy difference between low lying electronic states with different spin multiplicity [13].

We investigated the localization of the frontier orbitals. The spatial distribution of the frontier orbitals (HOMO) and (LUMO) provides a strategy by which the photovoltaic properties of phthalocyanine–fullerene supramolecule can be understood. We have opted to use hybrid functional (B3LYP) over Hartree–Fock (HF) method, as it can account for correlation effects also. Although (HF) describes exchange exactly, it results in unbound LUMO states. In the present calculations, well descriptions of the LUMO states are important, as the incoming electrons are assumed to pass through it. Therefore, the use of hybrid functional in DFT formalism is justified.

The definitions [14] for the isotropic polarizability is:

$$\alpha = \frac{1}{3}(\alpha_{xx} + \alpha_{yy} + \alpha_{zz}) \tag{1}$$

The polarizability anisotropy invariant is:

$$\Delta\alpha = \left[\frac{(\alpha_{xx} - \alpha_{yy})^2 + (\alpha_{yy} - \alpha_{zz})^2 + (\alpha_{zz} - \alpha_{xx})^2}{2}\right]^{\frac{1}{2}} \tag{2}$$

and the average polarizability is:

$$\beta_{\|} = \frac{1}{5}\sum_i (\beta_{iiz} + \beta_{izi} + \beta_{zii}) \quad (i \text{ from } x \text{ to } z) \tag{3}$$

Several successful applications using hybrid functionals have been reported [15]. The electronic absorption spectra require calculation of the allowed excitations and oscillator strengths. These calculations were carried out using TD-DFT with the (SDD) basis set and exchange correlation functional in vacuum. All calculations are of spin unrestricted type and carried out by using Gaussian 98 system [16]. The figures were generated by using the corresponding Gauss View software.

3. Results and discussions

3.1. The electronic structure and charges

The optimized geometries of the dyes D1–D5 are shown in Fig. 1 and the supramolecules S1–S5 are shown in Fig. 2. The optimal vertical distances between the donor (phthalocyanine) and acceptor (fullerene) in the supramolecules S1–S5 were calculated to be 4.18°, 2.57°, 2.56°, 2.57°, and 2.89A°, respectively. This order of distances implies that the strongest interaction between phthalocyanine and fullerene is assigned to the supramolecule S1, while the weakest interaction is assigned to the supramolecule S5. The peripheral tertiary butyl groups, with no π type electrons, are clearly not coplanar with the phthalocyanine ring. Since conjugation is very helpful for efficient electron transfer, the contribution of the peripheral tertiary butyl groups of a phthalocyanine ring to the process of electron transfer is restricted to their electron donating power.

Mulliken population analysis was performed in order to analyze the charge populations of the donor and acceptor units of the dyes and supramolecules. For this purpose we have performed single-point energy calculations on the optimized structures as the starting configurations. The charges on the phthaocyanine ring, metal, four tertiary butyl groups, and fullerene of the dyes D1–D5 and supramolecules S1–S5 are given in Table 1. The given data reveal that the metal and the four tertiary butyl groups of the dyes are the effective electron donor units, and the phthalocyanine rings are the effective electron acceptor units. The electron donating power of (La) is significantly greater than that of (Sc). While a negative charge is assigned to each N atom bonded to the metal in the metallophthalocyanine tertiary butyl ring, a positive charge is assigned to each N atom not bonded the metal in the same ring. Similar trends are observed for the supramolecules, but with a smaller transfer of electronic charge to the buckminster fullerene acceptor. However for the phthalocyanine–fullerene superamolecule, it is evident that no appreciable charge transfer occurs between the two building subunits. This indicates that there are some electrons transferred from the electron donor groups to the electron acceptor groups leading in turn to the formation of electron–hole pairs.

3.2. Frontier orbitals

The spatial distribution of the frontier orbitals provides a strategy by which the photovoltaic properties of molecular systems can be understood. Frontier orbitals isosurface plots are shown in Fig. 3 for the dyes, and in Fig. 4. for the supramolecules. The corresponding frontier orbital energies are given in Fig. 5 and Table 2. For dyes, while the highest occupied molecular orbitals (HOMOs) are π orbitals localized over the phthalocyanine rings, away from the tertiary butyl substituent groups, the lowest unoccupied molecular orbitals (LUMOs) are π^* orbitals localized over the central metal atoms. The HOMO–LUMO energy gap of the phthalocyanine ring becomes narrower under the effect of metal and tertiary butyl groups. This implies

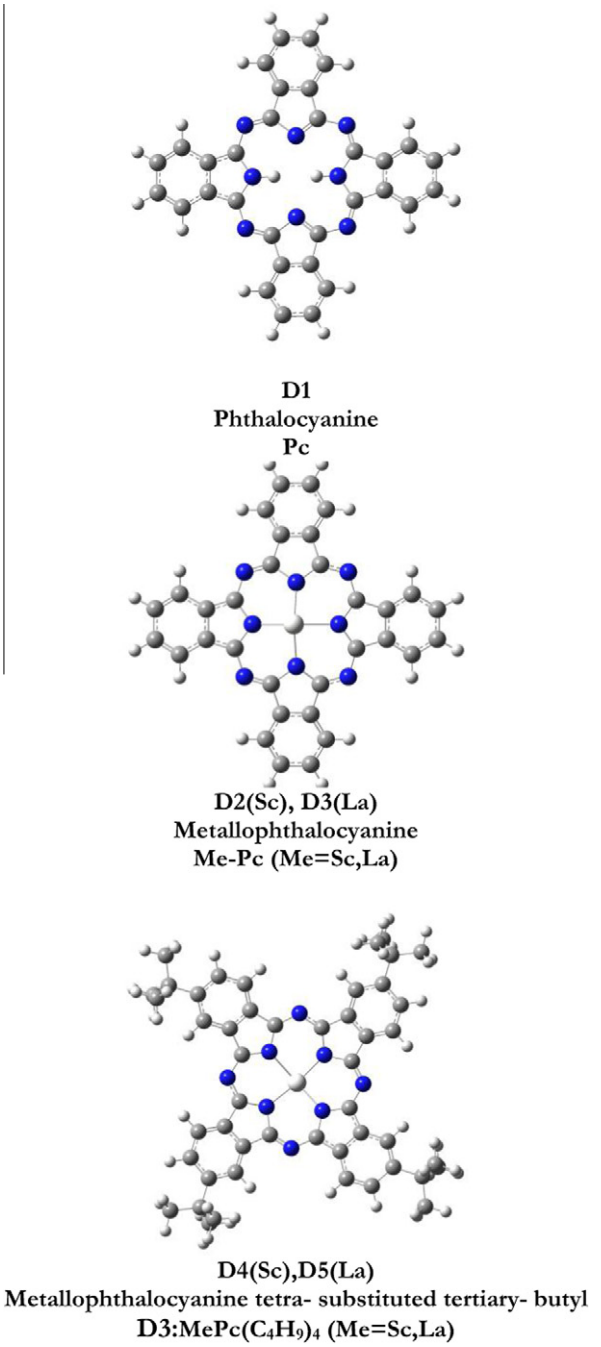

Fig. 1. Ball and stick representation of phthalocyanine dyes D1–D5: $(Me)_nPc(C_4H_9)_m$. Me:Sc,La; Pc: Phthalocyanine; C_4H_9: tertiary butyl; $n = 0, 1$, $m = 0, 4$.

that the density of states become more abundant near fermi levels. While the calculated HOMO and LUMO energies of the bare $Ti_{38}O_{75}$ cluster as a model for nanocrystalline material are −6.55 and −2.77 eV, respectively, resulting in a HOMO–LUMO gap of 3.78 eV, the lowest transition is reduced to 3.20 eV according to TDDFT, and this value is slightly smaller than typical band gap of TiO_2 nanoparticles with nanometer size [15]. Moreover, the HOMO, LUMO,

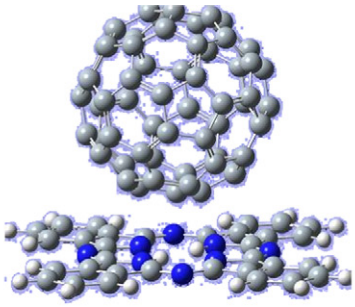

S1
Phthalocyanine-Buckminster Fullerene supramolecule
Pc.C_{60}

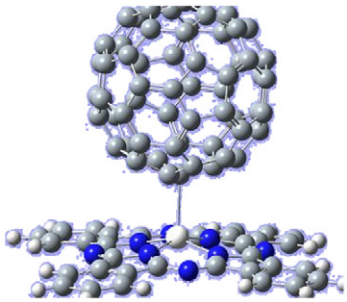

S2(Sc), S3(La)
Metallophthalocyanine-Buckminster Fullerene supramolecule
MePc.C_{60} (Me=Sc,La)

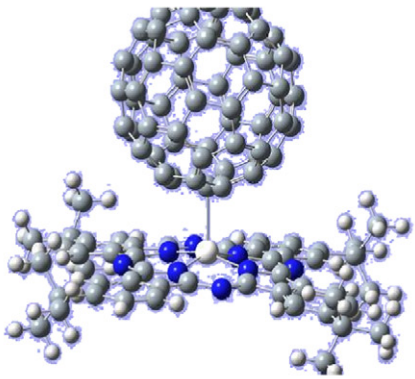

S4(Sc), S5(La)
Metallophthalocyanine-Buckminster Fullerene tetra substituted tertiary butyl supramolecule
MePc(C_4H_9)$_4$.C_{60} (Me=Sc,La)

Fig. 2. Ball and stick representation of Phthalocyanine–fullerene supramolecules S1–S5: $(Me)_nPc(C_4H_9)_m.C_{60}$Me:Sc,La; Pc: Phthalocyanine; C_4H_9: tertiary butyl; $n = 0, 1$; $m = 0, 4$.

and HOMO–LUMO gap of $(TiO_2)_{60}$ cluster is −7.52, −2.97, and 4.55 according to B3LYP/VDZ, respectively [17]. As shown in Fig. 6, the HOMOs of the dyes fall within the $(TiO_2)_{60}$ and $Ti_{38}O_{76}$ gaps. This data suggest the sensitized mechanism to be: interfacial electron transfer between the semiconductors $(TiO_2)_{60}$ and $Ti_{38}O_{76}$ electrodes and the dye sensitizers are electron injection processes from excited dyes to the semiconductors conduction bands. This is a kind of typical interfacial electron transfer reaction [18]. For the supramolecules Pc.C_{60}, ScPc.C_{60}, and

Table 1
Total charges of the dyes $(Me)_nPc(C_4H_9)_m$ and superamolecules $(Me)_nPc(C_4H_9)_m.C_{60}$ subunits computed at the B3LYP/SDD level of theory. Me:Sc,La; Pc: Phthalocyanine C_4H_9: tertiary butyl; $n = 0, 1$; $m = 0, 4$.

	ScPc	$ScPc(C_4H_9)_4$	LaPc	$LaPc(C_4H_9)_4$	$Pc.C_{60}$	$ScPc.C_{60}$	$ScPc(C_4H_9)_4.C_{60}$	$LaPc.C_{60}$	$LaPc(C_4H_9)_4.C_{60}$
Pc	−1.55	−1.23	−1.88	−1.52	0.00 (0.002)	−1.56	−1.21	−1.47	−1.29
Me:Sc,La	1.55	1.53	1.88	1.85		1.80	1.77	2.07	2.08
$(C_4H_9)_4$	–	−0.30	–	−0.33	–	–	−0.29	–	−0.26
C_{60}	–	–	–		0.00(−0.002)	0.22	−0.16	−0.60	−0.52

Values between round brackets are calculated at the M06/SDD level of theory for better description of non bonded interaction.

$ScPc(C_4H_9)_4.C_{60}$ the HOMOs are localized on the donors subunits and the LUMOs are localized on the acceptors subunits. However, for the supramolecules $LaPc.C_{60}$ and $LaPc(C_4H_9)_4.C_{60}$, both the HOMOs and LUMOs are localized on the donors and acceptor subunits simultaneously. The HOMO–LUMO energy gap of the supramolecule becomes narrower under the effect of metal and tertiary butyl groups. This implies that the density of states of the phthalocyanine–fullerene supramolecule become more abundant near the fermi level.

To understand the electron transport through the supramolecules, we have analyzed the frontier orbitals which provide a strategy by which the rectifying properties of these molecular systems can be understood. It has been suggested [19] that the potential drop ΔE_{LUMO} across each molecular rectifier is determined from the difference between E_{LUMO} and E_{LUMO+k} for an unoccupied orbital localized on the opposite (donor) side of the molecule from the LUMO. It is generally accepted that while the HOMO is localized on the donor, the LUMO is localized on the acceptor. Therefore, in a rectifying diode, the electrons are injected from the cathode to the LUMO state on the acceptor side. The incoming electron on the acceptor LUMO is then transferred to the lowest unoccupied orbital localized on the donor ring. Therefore if one can apply a bias voltage, the potential of which is E_{LUMO} (donor) − E_{LUMO} (acceptor), then the tunneling of electrons from one end to the other is possible [5]. From Fig. 4, it is clear that for the supramolecules, $LaPc.C_{60}$ and $LaPc(C_4H_9)_4.C_{60}$, the LUMOs are localized on the donors, thereby resulting in potential drops ($\Delta E_{LUMO} = E_{LUMO}$ (donor) − E_{LUMO} (acceptor)) of 1.05 eV for $LaPc.C_{60}$, and 1.29 eV for $LaPc(C_4H_9)_4.C_{60}$. The resulting potential drop of $LaPc.C_{60}$ thus increases by ca. 22.86% under the effect of the tertiary butyl groups. This significant increase in the potential drop indicates that the tertiary butyl complexes could be a better choice for the robust operation of the molecular rectifiers. In addition, the localized LUMOs on the donor, and the La atom also provide more channels for the electron transport from one side to the other.

3.3. Polarizability and hyperpolarizability

Polarizabilities and hyperpolarizabilities characterize the response of a system in an applied electric field. They determine the strength of molecular interactions as well as the cross sections of different scattering and collision processes. The potential of semiconducting organic materials to transport electric current and to absorb light in the UV–vis part of the solar spectrum is due to the sp^2-hybridization of carbon atoms. The electron in the p_z-orbital of each sp^2-hybridized carbon atom will form π-bonds with the neighboring p_z electrons. These π-electrons are of a delocalized nature, resulting in high electronic polarizability. Another important potential of semiconducting organic materials to transport electric current and to absorb light in the UV–vis part of the solar spectrum is the relatively small diffusion length of excitons [20]. These excitons are an important intermediate in the solar energy conversion process, and usually strong electric fields are required to dissociate them into free charge carriers, which are the desired final products for photovoltaic conversion. The relationships among the strong π-electron delocalization, high polarizability, strong electric field response, and photovoltaic conversion may now be clearer.

The present results indicate that the introduction of tertiary butyl groups to phthalocyanine leads to a simultaneous increase in polarizabilities, decrease in hyperpolarizabilities, and a higher photo-to-current conversion efficiency (red-shift of the UV maximum absorption bands). At one hand, this may be due to the fact that the length of the conjugated π bridge is not affected by the introduction of the tertiary butyl groups. At the other extreme, Anbarasau et al. [21] investigated the geometric, electronic structures, and electronic absorption spectra of silicon dichloride substituted phthalocyanine for dye sensitized solar cells. They found that the longer the length of the conjugate bridge in similar dyes, the larger the polarizability of the dye molecule, and the lower the photo-to-current conversion efficiency. They reported that this may be due to the fact that the longer conjugate π bridge enlarged the delocalization of electrons, thus it enhanced the response of the external field, but the enlarged delocalization may not be favorable to generate charge separated state effectively. So it induces the lower photo-to-current efficiency. We may note that Koyama et al. [22] examined the mechanisms of suppression and enhancement of photo-to-current conversion efficiency in dye sensitized sola-cells using carotenoid and chlorophyll derivatives as sensitizers. They found for a set of shorter polyene sensitizers having different polarizabilities, that the one with the highest polarizability (the highest trend of aggregate formation) exhibited the higher performance (photocurrent conversion efficiency) toward the lower dye concentration and the lower light intensity.

In order to investigate these relationships, the polarizabilities and hyperpolarizabilities of the dyes were calculated. Finite filed, sum over states method, and coupled perturbed Hartree–Fock method could be used to compute

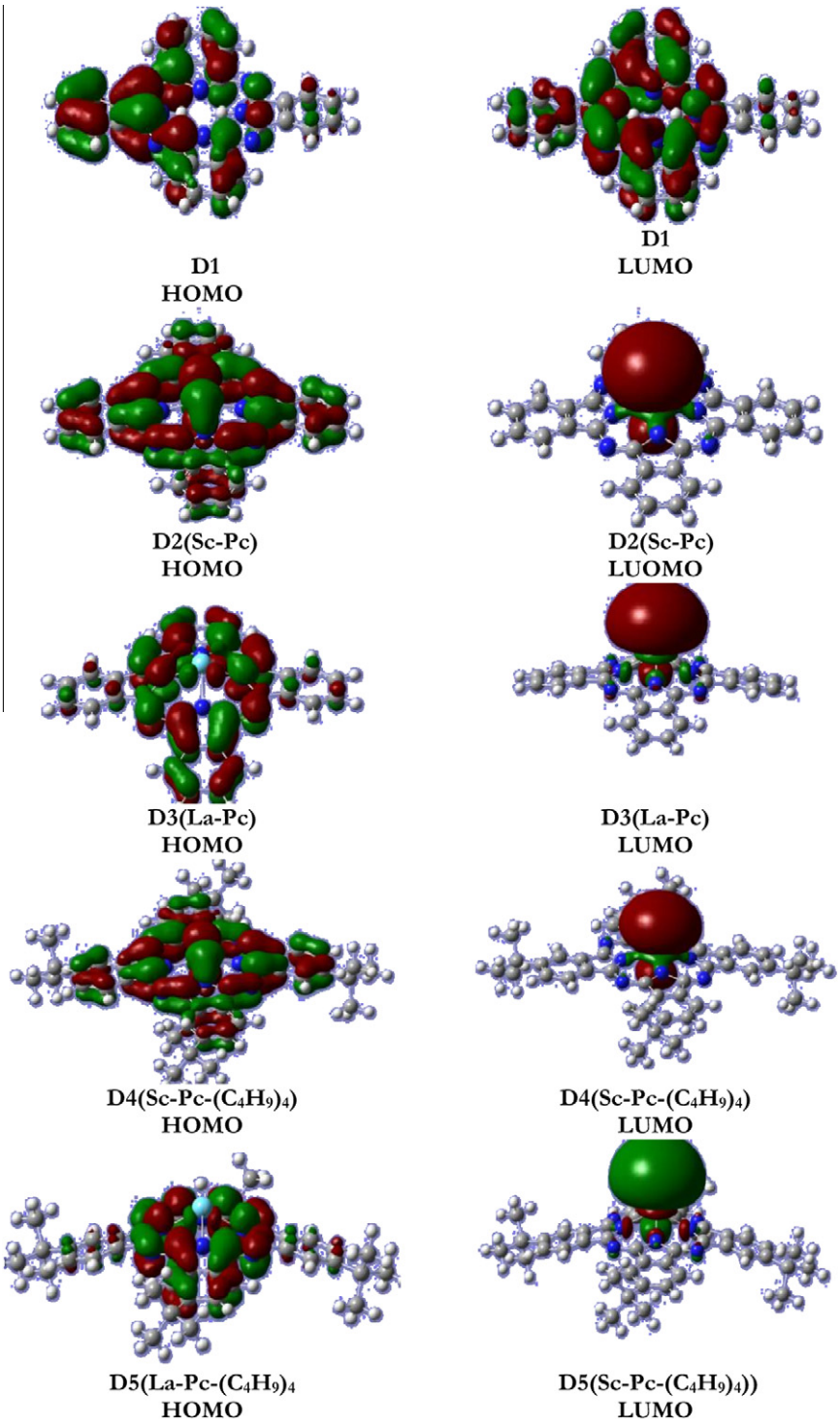

Fig. 3. Frontier orbital isosurface plots (isodensity contours = 0.02 a.u) of Phthalocyanine dyes computed at the B3LYP/LANL2MB level of theory.

polarizabilities and hyperpolaizabilities. However, the use of the previous methods with large sized basis sets for the dye molecules are too expensive. Here, we compute the polarizabilities and the first hyperpolarizabilities as a numerical derivatives of the dipole moment using B3LYP/SDD.

Table 3 lists the polarizabilities and hyperpolarizabilities of the dyes. In addition to the individual tensor components of the polarizabilities and the first hyperpolarizabilities, the isotropic polarizability, polarizability anisotropy invariant and hyperpolarizability are also calculated. The data of Table 3 suggest that the introduction of metal

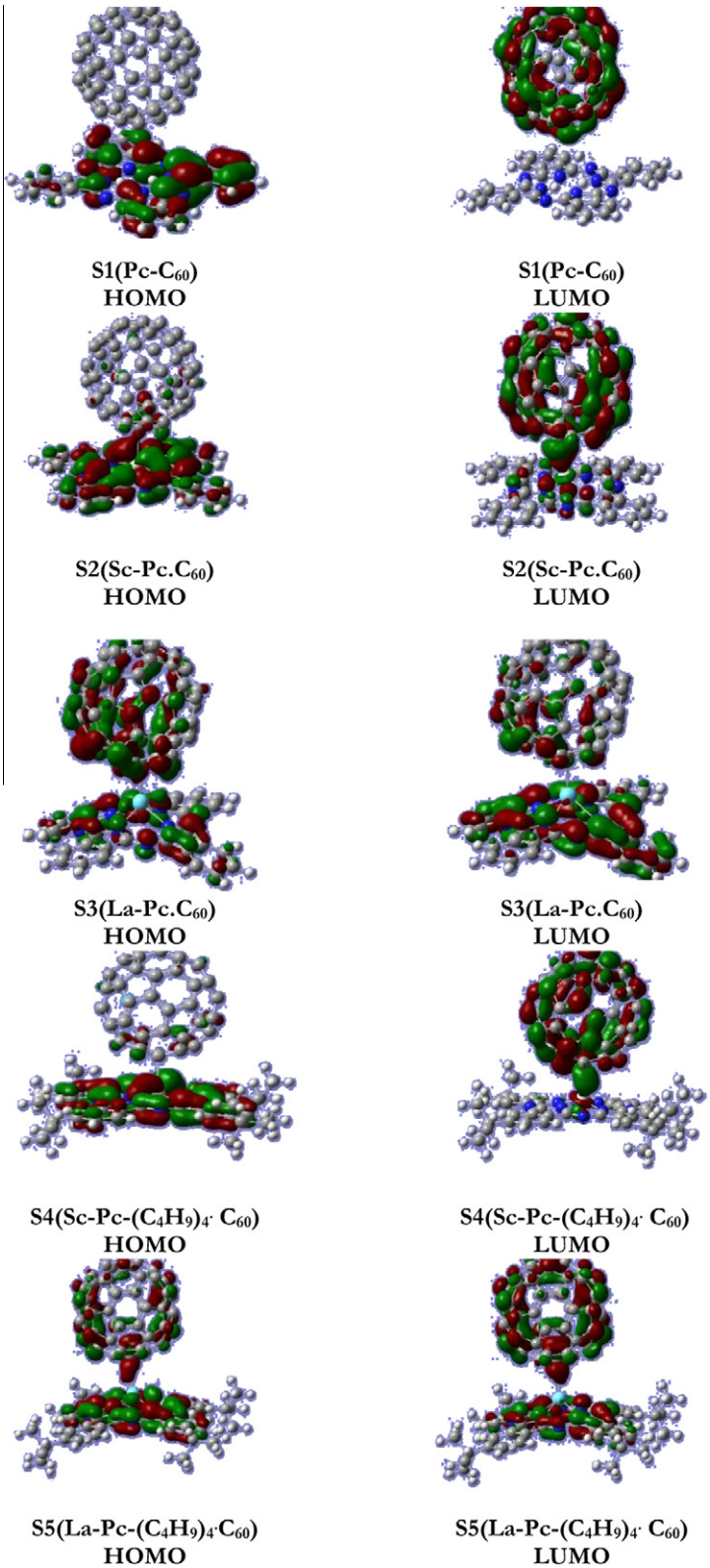

Fig. 4. Frontier orbital isosurface plots (isodensity contours = 0.02 a.u) of supramolecules S1–S5 computed at the B3LYP/LANL2MB level of theory.

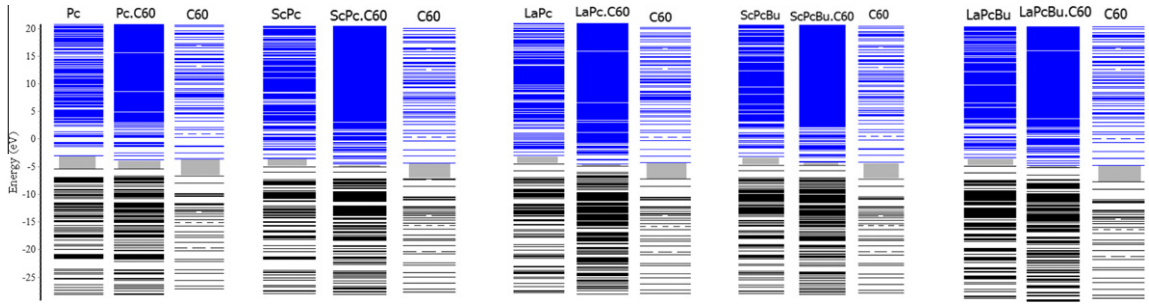

Fig. 5. Orbital energies(in eV) of the dyes $(Me)_nPc(C_4H_9)_m$, superamolecules $(Me)_nPc(C_4H_9)_m$.C60,and fullerene (C60) computed at the B3LYP/SDD level of theory. Me:Sc,La; Pc: Phthalocyanine; C4H9: tertiary butyl; $n = 0, 1$; $m = 0, 4$. (C4H9)4: Bu.

Table 2
Frontier orbital energies(in eV) of the dyes $(Me)_nPc(C_4H_9)_m$, superamolecules $(Me)_nPc(C_4H_9)_m$.C_{60},and fullerene (C_{60}) computed at the B3LYP/SDD level of theory. Me:Sc,La; Pc: Phthalocyanine; C_4H_9: tertiary butyl; $n = 0, 1$; $m = 0, 4$. $(C_4H_9)_4$: Bu.

	C_{60}	Pc	Pc.C_{60}	ScPc	ScPc.C_{60}	LaPc	LaPc.C_{60}	ScPcBu	ScPcBu.C_{60}	LaPcBu	LaPcBu.C_{60}
LUMO	−3.758	−3.04	−3.648 (−3.46)	−3.013	−3.886	−2.709	−4.09	−2.811	−3.799	−2.468	−3.762
HOMO	−6.743	−5.398	−5.419 (−5.58)	−4.523	−4.502	−4.16	−4.513	−4.312	−4.315	−3.918	−4.154
Band gap	2.985	2.358	1.771 (2.12)	1.51	0.616	1.451	0.423	1.501	0.516	1.45	0.392

Values between round brackets are calculated at the M06/SDD level of theory for better description of non bonded interaction.

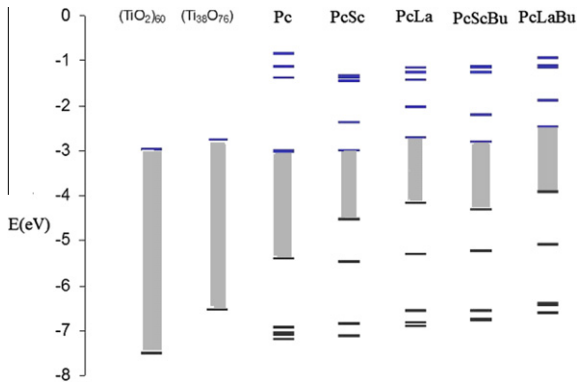

Fig. 6. HOMOs and LUMOs of (TiO2) and (Ti38O76) clusters, and the five HOMOs and five LUMOs of the dyes $(Me)_nPc(C_4H_9)_m$ computed at the B3LYP/SDD level of theory. Me: Sc, La; Pc: Phthalocyanine; C4H9: tertiary butyl; $n = 0,1$; $m = 0,4$. (C4H9)4: Bu.

atom and tertiary butyl groups to the phthalocyanine ring leads to a stronger response to the external electric field, and induces higher photo-to-current conversion efficiency.

3.4. The electronic absorption spectra

In order to understand the electronic transitions of the dyes, TD-DFT calculations on electronic absorption spectra in vacuum were performed, and the 10 lowest spin-allowed singlet–singlet transitions were taken into account. The results are shown in Table 4. The calculations were carried out at the B3LYP/SDD level of theory.

Primarily, the HOMO–LUMO energy gap of the phthalocyanine dye gets smaller under the effect of inserting the metal atoms and the tertiary butyl groups, Table 2, so it induces the red-shifts of the corresponding absorption bands, Table 4. The absorption in visible and near-UV regions is the most important region for photo-to-current conversion, so only the singlet to singlet transitions of the absorption bands with the oscillator strength larger than 0.01 and the wavelength longer than 300 nm were recorded in Table 4. The absorption band that corresponds to the maximum absorption of the phthalocyanine ring is red shifted by 474 and 347 nm under the effect of inserting Sc and La atoms respectively. The insertion of tertiary butyl groups causes additional red shifts of 31 and 20 nm to Sc and La complexes respectively. The present results indicate that the absorption bands of phthalocyanines are red shifted under the effect of substituents in consistence with pervious experimental data published for PcCu [23,24], PcFe(II) [25] and PcSi [26]. The maximum absorption bands near 573 and 920 nm of the simulated spectra of Pc and LaPc dyes, respectively, resulted from the electronic transitions from the initial states that are mainly contributed by the HOMOs to the final states that are mainly contributed by the LUMOs. These two absorption bands in the visible region are typical π–π^* transitions. In these transitions, while the initial and final states are related to the MOs that are localized in the phthalocyanine ring of the Pc dye, the initial state is localized in the phthalocyanine ring and the final state is localized in the central region of the metal of the LaPc dye, Fig. 3. The maximum absorption bands near 1047, 1078, and 940 nm of the dyes ScPc, $ScPc(C_4H_9)_4$, and $LaPc(C_4H_9)_4$, respectively resulted from the electronic transitions from the initial states that are mainly contributed by the HOMOs − 1 to the final states that are mainly contributed by the HOMOs. All other absorption bands of the dyes resulted from the electronic transitions from the initial states that are mainly contributed by the HOMOs − n. Usually, if the absorption bands are close to infrared

Table 3
Polarizabilities (α) and hyperpolarizabilitie(β) of the dyes $(Me)_nPc(C_4H_9)_m$ computed at the B3LYP/SDD level of theory. Me:Sc,La; Pc: Phthalocyanine; C_4H_9: tertiary butyl; $n = 0, 1$, $m = 0, 4$.

	α_{XX}	α_{XY}	α_{YY}	α_{XZ}	α_{YZ}	α_{ZZ}	α	$\Delta\alpha$
Pc	771.2	0.0006	758.5	0.0323	−0.0091	141.9	557.2	623.0
ScPc	887.8	−0.0122	794.1	−0.7504	0.0139	162.6	614.8	683.1
LaPc	791.5	0.059	849.3	−0.0044	5.0	199.6	613.5	622.8
*$ScPc(C_4H_9)_4$								
$LaPc(C_4H_9)_4$	1036.3	−1.3	1164.3	−0.374	0.6313	342.2	847.6	766.2

	β_{XXX}	β_{XXY}	β_{XYY}	β_{YYY}	β_{XXZ}	β_{XYZ}	β_{YYZ}	β_{XZZ}	β_{YZZ}	β_{ZZZ}	β_{II}
Pc	8447.6	−0.011	4341.7	0.6346	0.38	−0.0694	0.1321	8.7	0.0004	−0.005	0.304
ScPc	16676.5	−2.1	962.2	−0.4851	274.7	−0.0029	196.6	−6.4	0.0004	197	401
LaPc	−2.3	−490.1	−2.4	9744.2	881.2	0.043	613.7	−0.033	72.8	411.2	1144
*$ScPc(C_4H_9)_4$											
$LaPc(C_4H_9)_4$	−2.7	−19.7	−5.2	25.8	−555.8	26.0	−873.3	−0.8231	2.5	−366.2	−1077

* Convergence criterion is not met.

Table 4
Computed excitation energies, electronic transition configurations and oscillator strengths (f) for the optical transitions with $f > 0.01$ of the absorption bands in visible and near UV region for the dyes $(Me)_nPc(C_4H_9)_m$ computed at the B3LYP/SDD level of theory. Me:Sc,La; Pc: Phthalocyanine C_4H_9: tertiary butyl; $n = 0,1$; $m = 0,4$.

State	Excitation energy (eV/nm)	Configuration composition with lCI Coeff.l > 0.2 (corresponding transition orbital)	f
Pc			
1	0.689 (133 → 134)	2.17/573	0.3343
2	0.688 (133 → 135)	2.22/560	0.3816
3	−0.348 (130 → 135); 0.564 (132 → 135)	3.38/367	0.0816
7	−0.421 (131 → 135); 0.486 (132 → 134)	3.45/359	0.0476
8	−0.340 (130 → 135); 0.445 (131 → 134); −0.264 (132 → 135); 0.280 (133 → 136)	3.54/351	0.0318
HOMO is No. 133 orbital			
ScPc			
2	0.981 (137B → 138B)	1.18/1047	0.0936
6	0.808 (137A → 139A); −0.462 (137B → 139B); −0.207 (137B → 140B)	2.08/595	0.1628
8	−0.220 (137A → 140A); 0.787 (138A → 143A); 0.501 (138A → 148A)	2.36/525	0.0170
9	−0.632 (138A → 141A); 0.742 (138A → 145A)	2.38/522	0.0121
HOMO is No. 138 orbital			
LaPc			
2	−0.291 (147A → 150A); 0.947 (146B → 147B)	1.35/920	0.0849
5	0.835 (147A → 150A); 0.460 (147A → 152A); 0.204 (146B → 147B)	2.08/597	0.0895
6	0.702 (146A → 148A); 0.652 (147A → 151A); −0.222 (146B → 148B)	2.16/575	0.0484
7	−0.458 (146A → 148A); 0.656 (147A → 151A); −0.209 (145B → 147B); 0.444 (146B → 148B)	2.30/540	0.2307
8	−0.352 (147A → 150A); 0.861 (147A → 152A)	2.31/538	0.1465
HOMO is No. 147 orbital			
$ScPc(C_4H_9)_4$			
2	0.983 (201B → 202B)	1.15/1078	0.1095
6	0.822 (201A → 203A); 0.474 (201B → 203B)	2.04/608	0.1922
9	−0.417 (201A → 204A); −0.379(202A → 206A); 0.564 (202A → 207A); 0.530(202A → 208A)	2.35/527	0.0177
10	−0.565 (202A → 205A); 0.777 (202A → 209A)	2.36/525	0.0101
HOMO is No. 202 orbital			
$LaPc(C_4H_9)_4$			
2	0.960 (210B → 211B)	1.32/940	0.1244
5	0.909 (211A → 214A); 0.207 (211A → 215A); 0.321(211A → 216A)	2.01/617	0.0298
8	0.659 (210A → 212A); −0.421 (211A → 215A); 0.230 (209B → 211B); 0.500(210B → 212B)	2.31/537	0.3801
9	0.858 (211A → 216A); 0.221 (211A → 217A)	2.37/524	0.2613
HOMO is No. 211 orbital			

region, it is expected that the dyes have higher photo-to-current efficiency. On this basis, the ScPc and $ScPc(C_4H_9)_4$ dyes are expected to have the highest photo-to-current efficiencies. The given data indicate that the absorptions are photoinduced electron transfer processes. This implies that the corresponding excitations generate charge sepa-

Table 5
Theoretical data of free Sc atom and ScPc phthalocyanine dye. Ne: number of unpaired electrons. H: High spin. L: Low spin.

	Spin multiplicity	Spin state	Energy (a.u.)	ΔE^{H-L}_{atom}
Sc	2	L	−46.67411	1.083
	4	H	−46.63432	
			$Energy_{complex}$ (a.u.)	$\Delta E^{H-L}_{complex}$
ScPc	2	L	−1713.73235	0.740
	4	H	−1713.70517	

Table 6
computed excitation energies, electronic transition configurations and oscillator strengths (f) for the optical transitions with f > 0.01 of the absorption bands in visible and near UV region for the dyes ScPc in the high (4) and low (2) spin states computed at the B3LYP/SDD level of theory.

State	Configuration composition with lCI Coeff.l›0.2 (corresponding transition orbital)	Excitation energy (eV/nm)	*f*
Sc(4)Pc			
4	0.62 (138A → 141); 0.83 (139A → 142)	1.98/625	0.0103
10	0.71 (138A → 142A); 0.31 (139A → 141A); −0.56 (133B → 137B); 0.24 (136B → 139B)	2.25/551	0.0325
HOMO is No. 139 orbital			
Sc(2)Pc			
2	0.981 (137B → 138B)	1.18/1047	0.0936
6	0.808 (137A → 139A); −0.462 (137B → 139B); −0.207 (137B → 140B)	2.08/595	0.1628
8	−0.220 (137A → 140A); 0.787 (138A → 143A); 0.501 (138A → 148A)	2.36/525	0.0170
9	−0.632 (138A → 141A); 0.742 (138A → 145A)	2.38/522	0.0121
HOMO is No. 138 orbital			

rated states, and contribute to the sensitization of photo-to-current conversion processes. Insertion of metal atoms and substitution of tertiary butyl groups on the phthalocyanine moiety further shifts the absorption in these dyes and makes them potential candidates for harvesting light in the entire visible and near IR region for photovoltaic applications.

3.5. Magnetic spin quenching and UV–vis spectrum

The magnetic behavior of metals results from a competition between chemical bonding and magnetism, and is important to understand the role of the support. For example, the reactivity of adsorbed metal atoms will be different depending on whether the magnetic moment is quenched or not. When the free metal atom electronic configuration is $d^n s^2$, the resulting electronic configuration of the metal adatom may be expressed as $d^{n+1}s^1$ or even d^{n+2}. The strength of the metal-support interaction varies with the resulting d-population. This change in the electronic configuration of the metal in the support may result in a concomitant spin quenching with respect to the ground state multiplicity of the isolated metal atom. While the magnetic property of spin quenching in insulators has been investigated in some details [27] it is clearly overlooked for dye sensitizers in relation to the concept of photo-to-current conversion efficiency.

All of the previous calculations were carried out for the low spin state (2) of Sc and La in the phthalocyanine moieties. Sc is a representative of group IIIA transition metals with completely filled s-shell [Ar] $3d^1 4s^2$, and La is a representative of group IIIA lanthanides with completely filled s-shell [Ar] $5d^1 4s^2$. We have considered two electronic states for Sc, as a test case, to examine the spin quenching of this metal under the effect of the phthalocyanine ring, as well as the effect of the high spin stae (4) on the corresponding transition energies and UV–vis spectrum of the ScPc dye sensitizer. The Sc high spin state is (4), and the low spin is (2). The high (H) to low (L) spin transition energy of the free Sc atom was calculated from the relation:

$$\Delta E^{H-L}_{atom} = E^{H}_{atom} - E^{L}_{atom} \quad (4)$$

where E_{atom} is the electronic energy of the free Sc atom. In Table 5, the theoretical electronic configuration of Sc in the gas phase is given together with the corresponding number of unpaired electrons, spin multiplicity, spin state, electronic state, total electronic energy and the high to low spin transition energy. The present result of the high to low spin transition energy of free Sc atom at the B3LYP level of theory and SDD basis set is 1.083 eV. The positive sign indicates that the low spin state is favored. In other words, the low spin state of free Sc metal is more stable than the high spin state.It is interesting to compare the high-to low-spin transition energy of the free metal with the corresponding high-to low-spin transition energy of the metal in the phtalocyanine moiety. This comparison provides information on the change in the transition energy induced by the phthalocyanine ring, i.e., the energy required to go from the high to low-spin state when the support is present. Consequently our next discussion will be concerned with the spin transition energy of Sc in the selected ScPc dye sensitizer as well as the effect of the high spin state (4) on the transition energies and the UV–vis spectrum.The high (H) to low (L) spin transition energy of the Sc atom in ScPc complex was calculated from the relation

$$\Delta E^{H-L}_{complex} = E^{H}_{complex} - E^{L}_{complex} \quad (5)$$

where $E_{complex}$ is the total electronic energy of the complex. As shown in Table 5, upon interaction of Sc with the phthalocyanine ring, the sign of the high to low spin transition

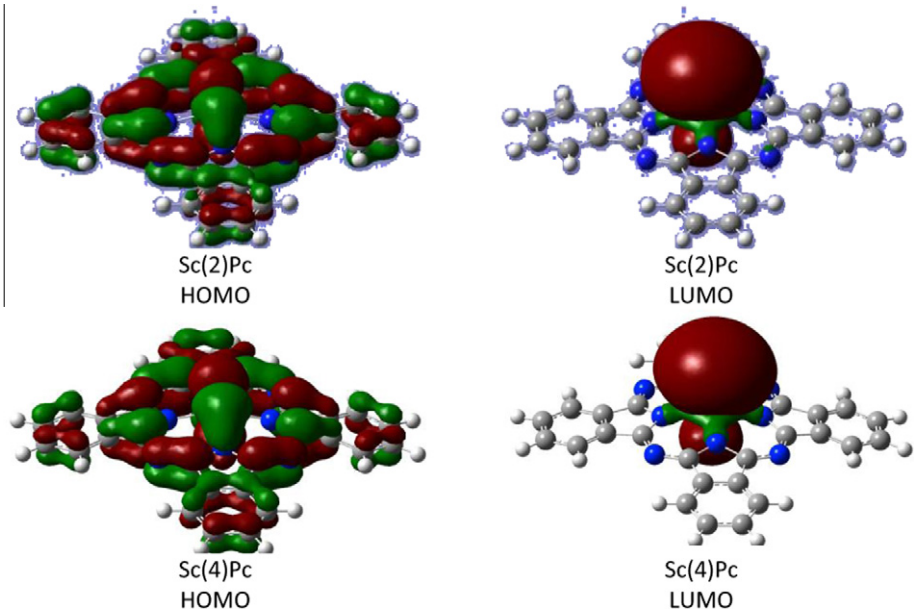

Fig. 7. Frontier orbital isosurface plots (isodensity contours = 0.02 a.u) and orbital energies(in eV) of the Phthalocyanine dye ScPc in the high (4) and low (2) spin states computed at the B3LYP/LANL2MB level of theory.

energies ΔE_{atom}^{H-L} calculated from relation (2) is still positive indicating that the spin states are preserved, and the low spin state is favored, i.e., the ground state of ScPc is doublet. However, the high to low spin transition energies was reduced by ca. 0.343 eV. The effect of the phthalocyanine ring is therefore significant, but still not enough to favor the high spin state.

In order to compare between the electronic transitions in the high (4) and low (2) spin states of the dye ScPc, we calculated the 10 lowest spin-allowed singlet–singlet transitions of the high spin state complex Sc(4)Pc. The results are shown together with the results of the low spin state complex Sc(2)Pc in Table 6, contour plots and energy levels in Fig. 7. The HOMO–LUMO energy gap of the Sc(4)Pc complex is −2.099 eV, compared with −1.294 eV for Sc(2)Pc complex, so it induces a blue shift to the corresponding absorption bands. The absorption band that corresponds to the maximum absorption of the high spin state complex Sc(4)Pc is blue shifted by 44 nm relative to the low spin state complex Sc(2)Pc. The maximum absorption band near 551 nm of the simulated spectrum of the high spin state complex Sc(4)Pc resulted from the electronic transitions from the initial state that is mainly contributed by the HOMO to the final state that is mainly contributed by the LUMO + 1. Other absorption bands resulted from the electronic transitions from the initial states that are mainly contributed by the HOMO − *n*. Since the absorption bands of the high spin state complex Sc(4)Pc are far from the infrared region, relative to the low spin state complex Sc(2)Pc, it is expected that the high spin state complex Sc(4)Pc has lower photo-to-current conversion efficiency. It turns out that the high spin state complex Sc(4)Pc is not a potential candidate for harvesting light in the visible and near IR region for photovoltaic applications.

The present results indicate that when the spin transition energy is significant, but not enough to quench the spin and favor the high spin state, the corresponding photo-to-current conversion efficiency is low. This result may be compared with the result of Koyama et al. [22] that the higher performance toward the lower dye concentration and the lower light intensity is ascribed to a decrease in the singlet–triplet (low spin to high spin) annihilation reaction. This result may also be compared with the finding of Shakaya et al. [28]. They examined the effect of applied magnetic field on photocurrent generation in poly-3-hexylthiophene:[6,6]-phenyl C61-butyric acid methyl ester photovoltaic devices, and found that the increase in photocurrent was attributed to an increase in the rate of intersystem crossing, between the singlet (low spin) and triplet (high spin) states leading to a high net efficiency of exciton dissociation.

4. Conclusions

The geometries, electronic structures, polarizabilities and hyperpolarizabilities, and UV–vis spectra of metallophthalocyanine dyes and metallophthallocyanine–fullerene supramolecules are investigated by using DFT and TD-DFT calculations. The calculated geometric characters indicate that the peripheral tertiary butyl groups, with no π type electrons, are not coplanar with the phthalocyanine ring. Since conjugation is very helpful for efficient electron transfer, the contribution of the peripheral tertiary butyl groups of a phthalocyanine ring to the process of electron transfer is restricted to their electron donating power. The sensitization mechanism is supported, and the introduction of metal atom and tertiary butyl groups induces higher photo-to-current conversion efficiency The high

spin state complex Sc(4)Pc is not a potential candidate for photovoltaic applications. In our opinion, the best candidate as a dye sensitizer for solar cells would be the electronic structure. The effect of present substituents (tertiary butyl groups, and metal atoms) on dye sensitization is reflected on the magnitudes of the band gaps and is confirmed by the calculated UV–vis spectra. It turns out that improving the nanoscale morphology together with the development of novel low band gap materials is still required to improve the power conversion efficiencies.

References

[1] A. Hagfeldt, M. Gratzel, Chem. Rev. 95 (1995) 49.
[2] (a) B. O'Regan, M. Gratzel, Naure 353 (1991) 737;
(b) M. Gratzel, Naure 414 (2001) 338;
(c) N.G. Park, K. Kim, Phys. Status Solidi A 205 (2008) 1895;
(d) Z.C. Rong, L.Z. Jiang, C.Y. Hong, C.H. Shan, W.Y. Zhi, Y.L. Hua, J. Mol. Struct.: THEOCHEM 899 (2009) 86.
[3] (a) A. Hagfeldt, M. Gratzel, Acc. Chem. Res. 33 (2000) 269;
(b) M. Gratzel, Inorg. Chem. 44 (2005) 6841.
[4] H. Mizuseki, N. Igarashi, R.V. Belosludov, A.A. Farajian, Y. Kawazoe, Synth. Met. 138 (2003) 281.
[5] C. Majumder, H. Mizuseki, Y. Kawazoe, J. Phys. Chem. A 105 (2001) 9454.
[6] R. Mosurkal, L. Hoke, S.A. Fossey, L.A. Samuelson, J. Kumar, D. Waller, R.A. Gaudiana, J. Macromol. Sci. 43 (2006) 1907.
[7] L. Sun, Fu.Q. Bai, Z.X. Zhao, H.X. Zhang, Sol. Energy Mat. Sol. Cells 96 (2011) 1800.
[8] Y. Zhang, X. Zhang, Z. Liu, Y. Bian, J. Jiang, J. Phys. Chem. A 109 (2005) 6363.
[9] Y. Zhan, L. Gan, D. Zhou, C.-H. Huang, J. Jiang, W. Liu, Solid State Commun. 106 (1998) 43.
[10] (a) A.D. Becke, J. Chem. Phys. 98 (1993) 5648;
(b) S.H. Vosko, L. Wilk, M. Nusair, Can. J. Phys. 58 (1980) 1200;
(c) A.D. Becke, Phys. Rev. A 38 (1988) 3098;
(d) C. Lee, W. Yang, R.G. Parr, Phys. Rev. B 37 (1988) 785.
[11] R. Caballol, O. Castell, F. Illas, J.P. Malrieu, I.P.R. Moreira, J. Phys. Chem. A 101 (1997) 7860.
[12] (a) A. Ricca, C.W. Bauschlicher, J. Phys. Chem. 98 (1994) 12899;
(b) T.V. Russo, R.I. Martin, P.J. Hay, J. Chem. Phys. 102 (1995) 8023;
(c) P.E. Siegbahn, R.H. Crabtree, J. Am. Chem. Soc. 119 (1997) 3103.
[13] a G. Pacchioni, The chemical physics of solid surfaces, in: D.P. Woodruff (Ed.), Oxide Surfaces, vol. 9, Elsevier, Amsterdam, 2001;
(b) G. Pacchioni, Surf. Rev. Lett. 7 (2000) 277.
[14] O. Christiansen, J. Gauss, J.F. Stanton, Chem. Phys. Lett. 305 (1999) 147.
[15] M.K. Nazeeruddin, F. De Angelis, S. Fantacci, A. Selloni, G. Viscardi, P. Liska, S. Ito, B. Takeru, M. Gratzel, J. Am. Chem. Soc. 127 (2005) 16835.
[16] M.J. Frisch et al., Gaussian 98, Gaussian Inc., Pittsburgh, PA, 1998.
[17] M.J. Lundqvist, M. Nilsing, P. Persson, S. Luell, Int. J. Quantum Chem. 106 (2006) 3214.
[18] D.F. Waston, G.J. Meyer, Annu. Rev. Phys. Chem. 56 (2005) 119.
[19] J.C. Ellenbogen, J.C. Love, Love, architectures for molecular electronic computers: 1. Logic structures and an adder designed from molecular electronic diodes, Proc. IEEE 8 (8) (2000) 386.
[20] P. Peumans, Y. Yakimov, S.R. Forrest, J. Appl. Phys. 93 (2003) 3693.
[21] P.M. Anbarasau, P.S. Kumar, M. Geether, R. Govindau, S. Monimegalai, K. Velmurugan, Recent Res. Sci. Technol. 2 (2010) 8.
[22] Y. Koyama, Y. Kakitani, H. Nagae, Molecules 17 (2012) 2188.
[23] S. Seelau, M.S. Agashe, D. Srinivas, S. Sivasanker, J. Mol. Catal. A: Chem. 16 (2001) 61.
[24] K.-J. Han, K.-Y. Kay, Bull. Korean Chem. Soc. 26 (2005) 1274.
[25] A. Zangvina, M. Bayo-Bangoura, K. Bayo, G.V. Guedraogo, Bull. Chem. Soc. Ethiop. 16 (2002) 73.
[26] J. Andzelm, A. Rawlett, J. Grlicki, J. Snyder, K. Baldridge, ART Aberdeen Proving Ground, MD 21005-5069, 2007.
[27] (a) A.S. Shalabi, M.M. Assem, K.A. Soliman, JMM 17 (2011) 3299;
(b) A.S. Shalabi, W.S. Abdel Halim, M.S. Ghonaim, Physica B 406 (2011) 397;
(c) A.S. Shalabi, W.S. Abdel Halim, N. Abdullah, Int. J. Quantum Chem., in press. http://dx.doi.org/10.1002/qua.23209.
[28] P. Shakaya, P. Desai, T. Kreowies, W.P. Gillin, S.M. Tuladhar, A.M. Ballantyne, J. Nelson, J. Phys, Condens. Matter 20 (2008) 452203.